IRIS AperTO

UNIVERSITÀ DEGLI STUDI DI TORINO

This is the author's final version of the contribution published as:

P.Tiberto, G.Barrera, F.Celegato, M.Coïsson, P.Rizzi, F.Vinai, A.C.Garcia Castro, L.Salamanca-Riba, R.D.Vispute, F.J.Espinoza Beltran, J.M.Sandaña

"Temperature dependence of magnetic and magnetotransport properties in BiFeO3 thin films by pulsed laser deposition"

Materials Research Society Symposium Proceedings, 1636 (2014) mrsf13-1636-u07-09 doi:10.1557/opl.2014.147

The publisher's version is available at:
http://dx.doi.org 10.1557/opl.2014.147

When citing, please refer to the published version.

iris-AperTO

University of Turin's Institutional Research Information System and Open Access Institutional Repository

Temperature dependence of magnetic and magnetotransport properties in $BiFeO_3$ thin films by pulsed laser deposition

P. Tiberto[1], G. Barrera[1,2], F. Celegato[1], M. Coïsson[1], P. Rizzi[2], F. Vinai[1], A.C. Garcia Castro[3], L. Salamanca-Riba[4], R.D. Vispute[4], F.J. Espinoza Beltran[3], J. Muñoz Sandaña[3]
[1]INRIM, Electromagnetism Division
strada delle Cacce 91, 10135 Torino (TO), Italy
[2]Università degli Studi di Torino, Dipartimento di Chimica
via P. Giuria 7, 10125 Torino (TO), Italy
[3]Unidad Queretaro, Centro de Investigacion y Estudios Avanzados del IPN
Queretaro, Mexico
[4]Materials Science and Engineering Department, University of Maryland
Baltimore, Maryland, USA

ABSTRACT

Multiferroic BFO/SRO/Si trilayers have been prepared by pulsed laser deposition in the form of thin films. As a function of the BFO layer thickness, magnetic and magneto-transport properties have been investigated at room temperature and down to 5 K. At low BFO layer thickness, a residual γ-Fe_2O_3 phase, which interacts interfacially with the SRO and BFO layers, is responsible for moderately hard magnetic properties of the film. On increasing BFO layer thickness, more homogeneous deposits are obtained with uniform magnetic and magneto-resistive properties.

INTRODUCTION

Multiferroic materials have been extensively studied in recent years because of their unique feature of combining multiple ferroic properties at the same time [1,2,3,4]. As an example $BiFeO_3$ (BFO) is a perovskite structure that is characterised by both ferroelectric and ferromagnetic properties at room temperature [5,6,7]. The possibility to control the orientation of the magnetisation in BFO systems using an electric field instead of a magnetic one makes them particularly interesting both for fundamental studies and for applications, especially in nanosructures, spintronics, and random access memories [8,9,10].

In this work, BFO thin films have been grown epitaxially on SRO underlayers by means of a pulsed laser deposition technique. Magnetic and magneto-resistance measurements have been used to investigate the role played by the BFO layer thickness on the magnetic properties of the bilayers. Inhomogeneities in the deposition at low BFO thickness and interfacial effects have been demonstrated to be significant in the room temperature and low temperature magnetisation reversal processes.

EXPERIMENT

$SrRuO_3$ (SRO) layers have been deposited on Si(100) substrates by means of a multi-target pulsed laser deposition (PLD) setup, exploiting a KrF laser with a wavelength of 248 nm, an impulse of 1 J/cm^2 with a duration of 20 ns and a repetition rate of 10 Hz. During the

deposition, the base pressure of the vacuum chamber was of the order of $1 \cdot 10^{-7}$ mbar and the O_2 pressure was of the order of 1 mbar. The substrate was heated at 650 °C. Subsequently, on top of the SRO layer, a $BiFeO_3$ (BFO) layer has been deposited with the same technique, starting from Bi_2O_3 and Fe_2O_3 targets. The thickness of the two layers for the studied samples is reported in Table I. The preparation conditions are the same for both SRO and BFO layers. After the deposition, the O_2 flow is interrupted and the chamber returns to its base pressure.

Sample	**$SrRuO_3$ thickness (nm)**	**$BiFeO_3$ thickness (nm)**
BFO5	145 ± 3	84 ± 4
BFO6	128 ± 5	144 ± 3
BFO4	137 ± 4	428 ± 3

Table I. SRO and BFO layers thickness for the three studied samples.

X-ray diffraction (XRD) has been measured in the grazing incidence configuration using the Cu-Kα radiation. The spectrum of sample BFO4 is shown in Figure 1. SRO and BFO peaks are identified.

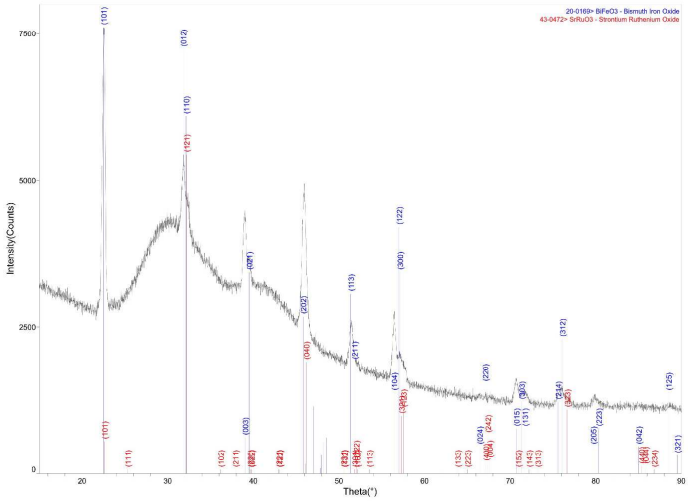

Figure 1. XRD spectrum of sample BFO4. Red labels: $SrRuO_3$ peaks. Blue labels: $BiFeO_3$ peaks.

SEM images have been acquired using secondary electrons and backscattered electrons in top-view or cross-section configuration. TEM structural characterisation has been performed with a Jeol 200 kV microscope in bright field and high resolution mode. Magneto-resistance measurements have been performed with the 4-contacts technique in a superconducting magnet with an applied field up to 70 kOe and at temperatures from 5 to 300 K. The contacts were made on the top surface of the BFO layer. The field was parallel to the sample plane and to the measurement current, whose value was fixed at 100 μA. Magnetic measurements have been performed with a Vibrating Sample Magnetometer (VSM), under a maximum field of 17 kOe, operating at room temperature and at low temperature (10 – 300 K) with a LHe cryostat. Magnetic force microscopy (MFM) has been performed at room temperature in intermittent-contact / lift mode using CoCr-coated tips at a distance of 90 nm from the sample surface.

DISCUSSION

Top-view secondary electrons SEM images of samples BFO5 and BFO4 are reported in Figure 2 (a) and (c) respectively. A matrix composed of small BFO grains is visible in all samples [12], whereas specimen BFO5 is also characterised by larger and flat platelets having a size between approximately 0.5 μm and ≈ 1.5 μm. In cross section (panels (b) and (d)), the SRO and BFO layers are clearly visible. The thickness values reported in table I have been determined from the available cross section images.

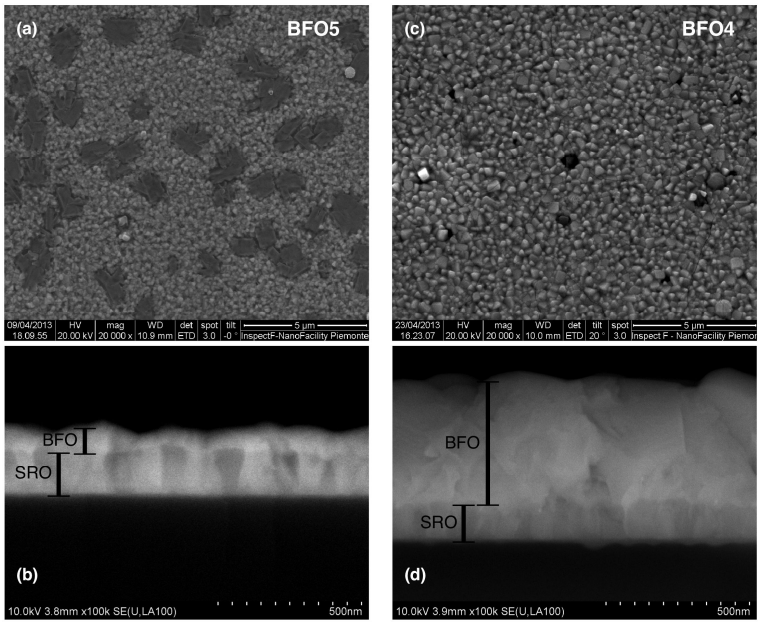

Figure 2. SEM images of selected BFO samples. (a) Top view of BFO5 sample, using secondary electrons. (b) Cross section view of BFO5 sample. (c) Top view of BFO4 sample, using secondary electrons. (d) Cross section view of BFO4 sample.

In order to identify crystalline phases constituting sample BFO5, and their orientation, a TEM lamella has been cut using a Focussed Ion Beam (FIB) process and detached from the thin film. Subsequently the lamella has been observed in a scanning electron microscope using backscattered electrons (Fig. 3a) and in a TEM (Fig. 3b). From SEM cross section analysis, the presence of a layer about 140 nm thick of SRO was observed, constituted by columnar crystals about 60 nm diameter, on which two phases with different contrast were observed (Fig. 3a). The darker one was identified as γ-Fe_2O_3 from lattice fringes present in High Resolution TEM analysis, although the presence of Fe_3O_4, as documented in some literature [13], cannot be excluded; it appears, from top view SEM observations (Fig. 1a), to be faceted with plate-like shape, about 50 nm thick and between 0.5 μm and 1.5 μm large. The brighter phase was determined to be BFO from EDS analysis and relative colour intensity analysis of the SEM images in backscattered electrons. In Fig 3 (a), it is evident that the contrast of the BFO phase changes when crystals are in contact with γ- Fe_2O_3 (red cicles in Fig 3a). This could be related to local changes in concentration of the elements during the deposition process. An excess of iron

can locally lead to an increase of the concentration of this element during the formation of BFO phase. Therefore, a compositional gradient can be expected depending on the area in which BFO crystals nucleate during deposition. TEM bright field images (Fig. 3b) show that BFO crystals about 80 nm thick grow epitaxially with respect to the SRO underlayer. Conversely, γ-Fe_2O_3 platelets do not grow epitaxially. Both γ-$Fe_2O_3$and BFO are uniformly distributed on the sample surface.

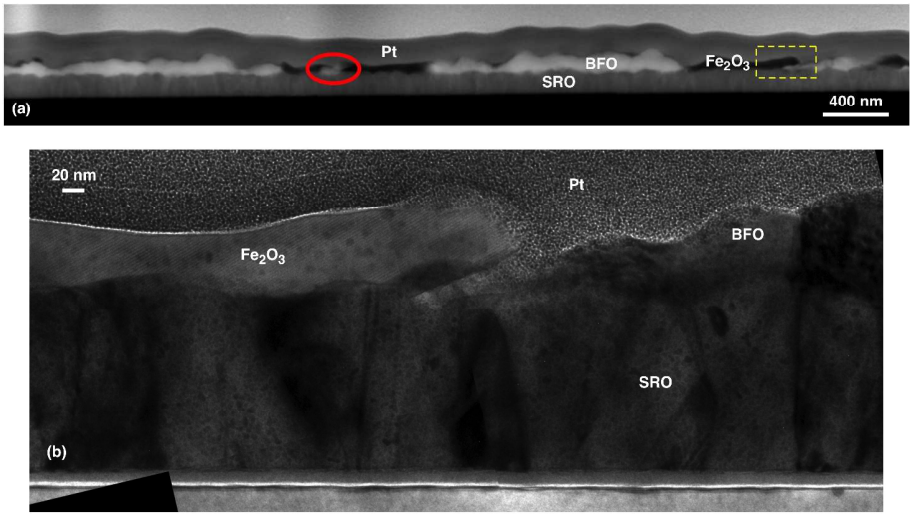

Figure 3. (a) Backscattered electrons SEM image of a lamella cut from sample BFO5. SRO, BFO and γ-Fe_2O_3 are indicated. (b) TEM bright field image of the area shown in panel (a). Pt was added to the sample during the FIB production of the lamella.

The same morphology has been observed by means of atomic force microscopy, as shown in Fig. 4. The corresponding MFM images show that the BFO phase has no magnetic contrast, as expected being BFO antiferromagnetic at room temperature. The granular structure visible in the MFM image of sample BFO4 is due to direct interaction with the sample surface, as evidenced by the strong correlation with the morphology, and does not have a magnetic origin. Conversely, the γ-Fe_2O_3 platelets that are present in sample BFO5 are characterised by a well defined magnetic contrast, that can be associated to moderately hard magnetic properties.

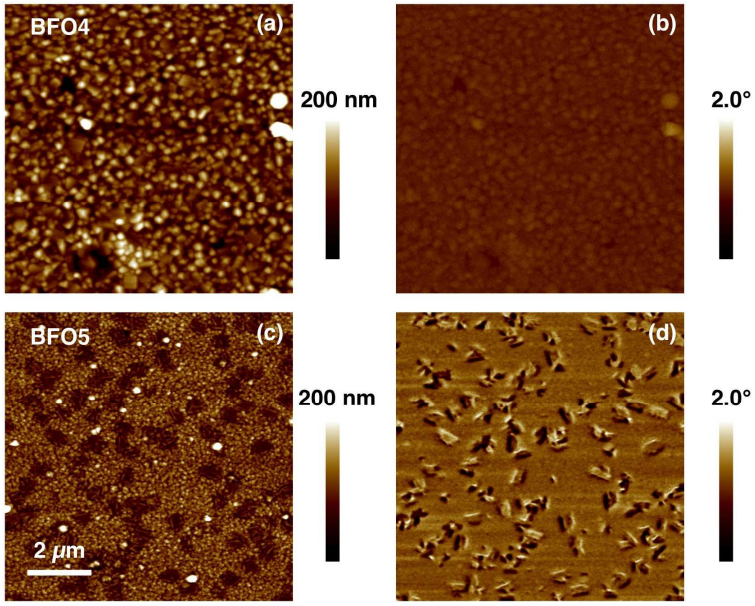

Figure 4. (a) AFM image of sample BFO4. (b) Corresponding MFM image, phase channel. (c) AFM image of sample BFO5. (d) Corresponding MFM image, phase channel.

These results are confirmed by the room temperature hysteresis loops measured with the VSM, that are reported in Fig. 5. The loops are normalised to the saturation. Samples BFO4 and BFO6 display a very weak magnetic moment (reflected in the more noisy signal), that can be attributed to uncompensated moments of the BFO sublattices due to canted spins arising from the Dzyaloshinskii-Moriya interaction [3,4] or the the presence of a parasitic Fe_2O_3 phase [11]. Conversely, sample BFO5 has a much stronger magnetic moment, that is the sum of a similar contribution coming from the BFO layer and of the magnetisation of the γ-Fe_2O_3 platelets. These are responsible for the hard magnetic phase of the BFO5 loop, as shown in Fig. 5 (right panel). Additionally, a contribution of Fe diffusion in the BFO or SRO layers at the interfaces with the γ-Fe_2O_3 platelets, giving rise to the loop shape observed in Fig. 5b, cannot be ruled out [15].

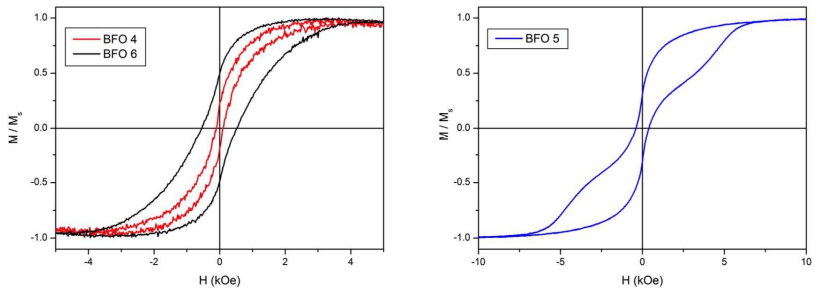

Figure 5. Left panel: room temperature normalised hysteresis loops of samples BFO4 and BFO6. The magnetic field is applied in the sample plane. Right panel: room temperature normalised hysteresis loop of sample BFO5. Note the different horizontal scale.

As the temperature is lowered, a new contribution to the magnetic signal appears below the transition temperature of the SRO layer, that becomes ferromagnetic below ≈ 160 K [16]. This is particularly clear in the FC/ZFC curves reported in Fig. 6 for samples BFO5 and BFO6. Independent of the presence or not of the γ-Fe_2O_3 platelets, in fact, these M vs. T curves display a transition that can be attributed to the SRO layer approaching the temperature at which its crystalline cell reversibly changes configuration and its magnetic properties are suddenly modified. Moreover, below ≈160 K the magnetisation of SRO has been reported to be enhanced by interface interactions with the capping BFO layer [12]. The transition is evident in the FC curve, where the magnetic moment of the SRO layer reduces to zero at a temperature of ≈ 175 K. The remaining magnetic signal is due to the BFO layer whose residual ferromagnetism is responsible for the hysteresis loops of Figure 6. In sample BFO5, the γ-Fe_2O_3 platelets are responsible for an even larger magnetic moment because of their ferromagnetic nature up to at least room temperature. In the ZFC curves the SRO transition is marked by a non monotonous behaviour of the M vs. T curve possibly due to an initial orientation of the magnetisation of both sublattices along the direction of the applied field that gives rise to the magnetisation increase, followed by the drop to zero when the transition temperature is approached. In sample BFO5 a small peak pointing downward may be associated to an exchange coupling interaction between the γ-Fe_2O_3 platelets or the BFO layer and the weak magnetic moment of the SRO very close to its transition temperature [14].

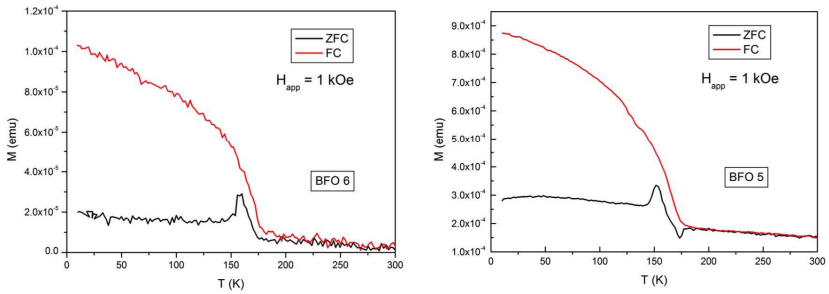

Figure 6. Field cooled and Zero field cooled measurements at 1 kOe of samples BFO6 (left panel) and BFO5 (right panel).

However, the lowering of the temperature affects the magnetic properties of the γ-Fe_2O_3 grains as well, as seen in the hysteresis loops reported in Fig. 7 for the BFO5 sample. At 150 K, therefore below the transition temperature of SRO, the loop begins changing shape, acquiring a progressively more pronounced hysteresis. The appearance of anomalous magnetic properties of BFO at these temperatures can not be ruled out, and could contribute to the overall loop shape [17]. Below 100 K the anisotropy field is larger than the maximum applied field, therefore the measured curves are minor loops, that are shifted in the second quadrant because the applied field is too weak. Even in this case, however, a two-phase behaviour can be observed, with the γ-Fe_2O_3 grains being responsible for most of the measured magnetic moment, and being affected by the interaction with the SRO layer underneath, that induces in them a much harder magnetic response.

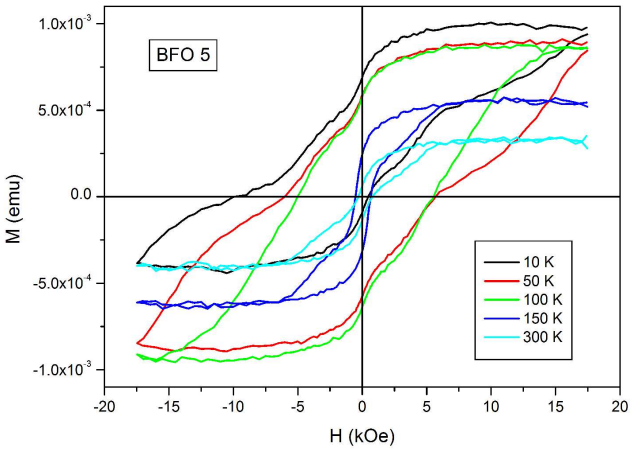

Figure 7. Low temperature hysteresis loops of sample BFO5.

To further investigate the complex magnetic behaviour of the studied samples, magneto-resistance measurements have been performed with the 4-contacts technique on all samples. The contacts are made with silver paint on top of the BFO layer. BFO is an insulator, but it is often subject to high leakage currents [18,19,20]. Indeed, an electrical current can be injected through the BFO layer in the conductive SRO [21], giving rise to a non metallic behaviour of the junction, as expected (Fig. 8). Once the current is injected in the SRO layer, a weak magneto-resistance signal can be observed in all samples at low temperature, that quickly disappears being overcome by the noise. As an example, the MR curve of sample BFO4 at 5 K is reported in Fig. 9 (right panel). Conversely, sample BFO5 is characterised by a richer MR behaviour,where the hysteretic shape of the MR curves is progressively reduced until a parabolic shape is reached above the transition temperature of SRO (Fig. 9 left panel). Since the γ-Fe_2O_3 grains are directly deposited on top of the SRO layer, the conduction electrons can diffuse in the Fe-rich phase and provide an additional contribution to the magneto-resistance of the sample. BFO/y-Fe2O3 heterostructures have been shown to display enhanced ferroic properties [22], therefore confirming the improvement of the physical characteristics of these systems that are promising for perspective applications.

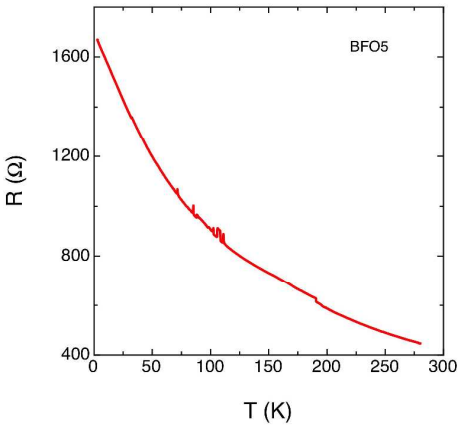

Figure 8. Electrical resistance vs. temperature of sample BFO5.

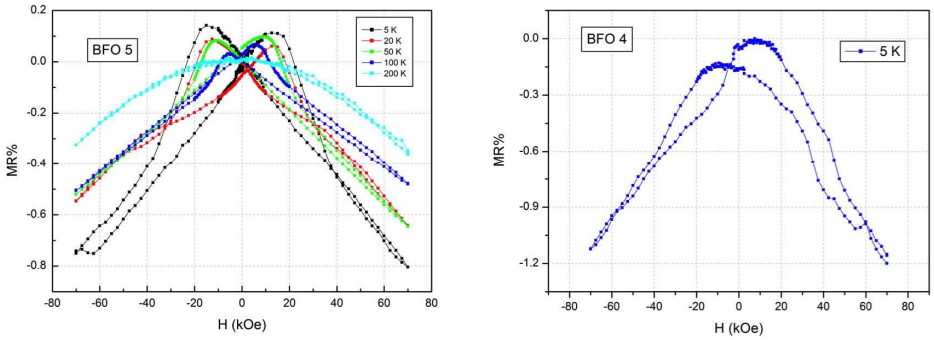

Figure 9. Left panel: selected MR curves of sample BFO5 at low temperature. Right panel: MR curve of sample BFO4 at 5 K.

CONCLUSIONS

The magnetic and magneto-transport properties of Si/SRO/BFO thin films have been investigated as a function of the BFO layer thickness. At high BFO thickness the system is characterised by an almost antiferromagnetic BFO layer and no significant magnetic and magneto-resistance properties are observed at room temperature or low temperature. Conversely, when the BFO thickness is progressively reduced, weak magnetic properties appear that can be attributed to canted spins. Further reduction of the BFO thickness determines the appearance of a non uniform structure, characterised by a BFO matrix in which γ-Fe_2O_3 platelets are dispersed. The interaction with BFO and SRO at their interface enhances the coercivity of the platelets, that turn out to display a moderately hard magnetic behaviour, that is severely reinforced below the temperature at which the SRO underlayer becomes ferromagnetic. Magneto-resistance measurements, exploiting the metallic conductivity of SRO and the high leakage currents of BFO, support the magnetic measurements indicating a magnetic behaviour of the γ-Fe_2O_3 platelets that is affected by the interaction with the surrounding phases.

ACKNOWLEDGMENTS

The Authors would like to acknowledge the EC FP7 Grant No. 263878 (BisNano) project.

REFERENCES

1. C. Binrk, X. He, Y. Wang, S. Sahoo, Christian Binek Publications 65 (2008) 1-9
2. M. Fiebig, J. Phys. D 38 (2005) R123
3. S.W. Cheong, M. Mostovoy, Nature Mater. 6 (2007) 13
4. R. Ramesh, N.A. Spaldin, Nature Mater. 6 (2007) 21
5. J. Wang, J.B. Neaton, H. Zheng, V. Nagarja, S.B. Ogale, B. Liu, D. Viehland, V. Vaithyanathan, D.G. Schlom, U.V. Waghmare, N.A. Spaldin, K.M. Rabe, M. Wuittig, R. Ramesh, Science 299 (2003) 1719

6. G. Catalan, J.F. Scott, Adv. Mater. 21 (2009) 2463-2485
7. D. Sando, A. Agbelele, D. Rahmedov, J. Liu, P. Rovillain, C. Toulouse, I.C. Infante, A.P. Pyatakov, S. Fusil, E. Jacquet, C. Carrétéro, C. Deranlot, S. Lisenkov, D. Wang, J.-M. Le Breton, M. Cazayous, A. Sacuto, J. Juraszek, A.K. Zvezdin, L. Bellaiche, B. Dkhil, A. Barthélémy, M. Bibes, Nat. Mater. 12 (2013) 641-646
8. V.B. Naik, R. Mahendiran, Solid State Comm. 149 (2009) 754-758
9. P. Ravindran, R. Vidya, A. Kjejshusm H. Fjellvag, Phys. Rev. B 74 /2006) 224412-224429
10. V.A. Khomchenko, D.A. Kiselev, M. Kopcewicz, M. Maglione, V.V. Shvartsman, P. Borisov, W. Kleemann, A.M.L. Lopese, Y.G. Pogorelov, J.P Araujo, R.M. Rubinger, N.A. Sobolev, J.M. Vieira, A.L. Kholkin, J. Magn. Magn. Mater. 321 (2009) 1692-1698
11. H. Béa, M. Bibes, A. Barthélémy, K. Bouzehouane E. Jacquet, A. Khodan, J.-P. Contour, S. Fusil, F. Wyczisk, A. Forget, D. Lebeugle, D. Colson, M. Viret, Appl. Phys. Lett. 87 (2005) 072508
12. C. Ostos, O. Raymond, N. Suarez.Almodovar, D. Bueno.Baqués, L. Mestres, J.M. Siqueiros, J. Appl. Phys. 110 (2011) 024114
13. E.-Mi Choi, E. Weal, Z. Bi, H. Wang, A. Kursumovic, T. Fix, M.G. Blamire, J.L. MacManus-Driscoll, Appl. Phys. Lett. 102 (2013) 012905
14. L. Wang, Z. Wang, K.-J. Jin, J.-Q Li, H.-X. Yang, C. Wang, R.-Q. Zhao, H.-B. Lu, H.-Z. Guo, G.-Z. Yang, Appl. Phys. Lett. 102 (2013) 242902
15. T. Hussain, S.A. Siddiqi, S. Atiq, M.S. Awan, Progr. Nat. Sci.: Mater. Internat. 23 (2010) 487-492
16. T. Kiyama, K. Yoshimura, K. Kosuge, Phys. Rev. B 54 (1996) R756-R759
17. J. Lu, A. Günther, F. Schrettle, F. Mayr, S Krohns, P. Lunkenheimer, A. Pimenov, V.D. Travkin, A.A. Mukhin, A. Loidl, Eur. Phys. J. B 75 (2010) 451-460
18. S. Greicius, J. Banys, I. Szafraniak-Wiza, Proc. Appl. Ceramics 3 (2009) 85-87
19. H. Zhu, S. Wang, P. Jiang, J. Shen, W. Tang, J. Kor. Phys. Soc. 57 (2010) 268-271
20. A. Lahmar, S. Habouti, C.-H- Solterbeck, N. Es-Souni, B. Alouadi, J. Appl. Phys. 105 (2009) 014111
21. N.D. Zakharov, K.M. Satyalakshmi, G. Koren, D. Hesse, J. Mater. Res. 14 (1999) 4385-4394
22. O. Gautreau, C. Harnagea, L. Gunawan, G.A. Botton, L. Pintilie, M.P. Singh, A. Pignolet, J. Appl. Phys. 108 (2010) 114111